THE JOURNAL OF PHYSICAL CHEMISTRY B

Article

pubs.acs.org/JPCB

The Interpretation of Diffraction Patterns of Two Prototypical Protic Ionic Liquids: a Challenging Task for Classical Molecular Dynamics Simulations

Lorenzo Gontrani,[†,‡,*] Enrico Bodo,[‡,*] Alessandro Triolo,[†] Francesca Leonelli,[‡] Paola D'Angelo,[‡] Valentina Migliorati,[‡] and Ruggero Caminiti[‡]

[†]Consiglio Nazionale delle Ricerche, Istituto di Struttura della Materia, Area della ricerca Roma Tor Vergata, Via del Fosso del Cavaliere, I-00133 Roma, Italy

[‡]Dipartimento di Chimica, Università di Roma, "La Sapienza", P. le Aldo Moro 5, I-00185 Roma, Italy

Supporting Information

ABSTRACT: In this study, we discuss the performance of classical molecular dynamics in predicting the experimental X-ray diffraction patterns of liquid ethylammonium nitrate (one of the simplest protic room-temperature ionic liquid showing amphiphilic behavior) and of its hydroxy derivative (2-ethanolammonium nitrate, 2-HOEAN). Newly recorded energy-dispersive X-ray diffraction structure factors are compared with the corresponding quantities extracted from molecular dynamics simulations. Other useful theoretical and experimental indicators are used as a probe of the local structure of the title ionic liquids. We shall show that the use of a general purpose, two-body terms only, force field, such as OPLS/AA is able to describe most of the structural experimental data. However, we shall also point out that an improved description of some key structural features observed in the X-ray radial distribution function, can be obtained very easily by adding a general three-body potential energy term instead of changing the two-body potential parameters, in order to optimize the agreement with experimental data. This three-body term turns out to be naturally able to describe the complex polarization effects due to hydrogen bonding without requiring a quanto-mechanical treatment or a polarizable force field. In addition the present model turns out to be able to account for the presence of a low-Q peak in the scattering patterns of EAN, which has been commonly interpreted as a manifestation of the amphiphilic nature of this compound.

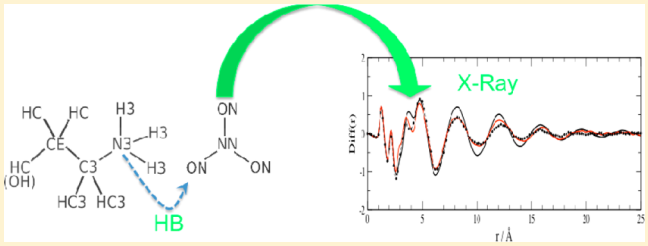

INTRODUCTION

Among all the innovative materials developed in the last 20 years, ionic liquids (ILs), represent an especially intriguing class of compounds, since they show a series of remarkable properties that attracted the attention of the research community for both academic and applicative issues. Besides the fact that their negligible vapor pressure makes them ideal candidates to replace the traditional noxious volatile organic compounds thereby prompting their use as "green solvents", the possibility of modulating their physicochemical properties by changing, even slightly, the chemical structure of the constituting ions has allowed their use in many industrial and technological processes, whose number is everyday increasing. Cellulose processing,[1,2] nuclear fuel recovery,[3,4] and transport of reacting gases,[5−7] are only some of the most notable applications.

ILs peculiar properties stem from the complexity of the nanoscopic interactions between their molecular constituents that include both long-range isotropic Coulombic forces and short-range van der Waals ones. In addition, many ionic liquids are also characterized by the presence of anisotropic hydrogen bonds.[8]

In this study, we focus our attention on protic ionic liquids (PILs) that are obtained from the proton transfer reaction between a Brønsted acid and a Brønsted base. Two short-chain representatives of this class of materials are considered, ethylammonium nitrate (EAN), and ethanolammonium nitrate (HOEAN; IUPAC name, 2-hydroxyethanaminium nitrate; CAS, 20748-72-5; CHEBI, 63878), EAN hydroxy derivative (see Chart 1). These two liquids are actually the oldest low-melting fused salts ever synthesized (EAN: Walden, 1914;[9] HOEAN: Gabriel, 1888[10]); EAN is a liquid at room temperature, while HOEAN melts at about 55 °C, but can be undercooled as a liquid down to about −25 °C.[11]

In contrast to the more common aprotic ionic liquids (AILs), PILs cations and anions are (in principle) in equilibrium with the conjugated nonionic species. The concentration of neutral species is often negligible in the liquid,[12] even though it can be sometimes measured. For neat liquid EAN, in particular, Kanzaki et al.[13] studied the autoprotolysis process

Received: June 21, 2012
Revised: October 10, 2012
Published: October 11, 2012

dx.doi.org/10.1021/jp306110g | J. Phys. Chem. B 2012, 116, 13024−13032

Chart 1. Structure and Atom Types (To Be Used in the Molecular Dynamics Simulation) of Ethylammonium (Left), and Nitrate (Right)

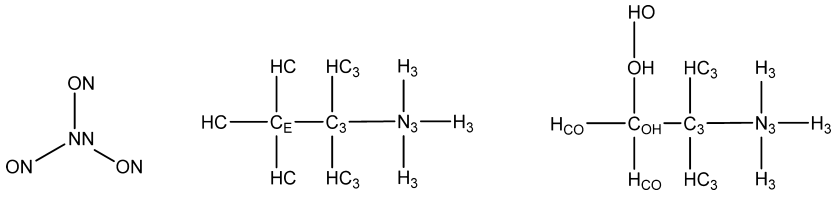

$$C_2H_5NH_3^+NO_3^- \rightleftharpoons C_2H_5NH_2 + HNO_3$$

with potentiometric methods, reporting a value of 10^{-10} mol^2 dm^{-6} for the equilibrium constant. Although PILs, owing to the cited equilibrium, can lack one of the most renowned features of AILs, namely the negligible vapor pressure,[14] the interest in these systems by the scientific community has grown very fast in recent years. Their protic nature, both as donors and as acceptors, in fact, makes them capable of forming hydrogen bond networks. This property, for instance, has made EAN one of the first-choice crystallizing agents for proteins.[15] For their amphiphilic and highly polar character,[16] PILs find many applications in organic synthesis, liquid–liquid chromatography, as proton conductors in fuel cells,[17] self-assembly media,[18] catalysts,[19] propellants,[20] and explosives,[21] as well as refolding agents for proteins.[22]

Given the great technological importance of these compounds, the number of experimental investigations aimed to assess their structural features has grown rapidly in the last five years. In a large number of studies, researchers by the group of Atkin and Warr[23−25] and by the group of Drummond and Greaves[26−28] have described in detail many aspects of their nanostructural and interfacial properties, with particular attention to self-assembly materials, using small angle X-ray and neutron diffraction and reflectivity, as well as microscopy. A noteworthy result is the observation that although EAN has a short alkyl chain, in the neutron diffraction pattern (see, e.g., the *N*-methyl deuterated samples in ref 23, the figures reported in ref 24, and our own measurements on protiated EAN reported below), low Q diffraction features are found at Q = 0.66 $Å^{-1}$ (EAN) and 0.76 $Å^{-1}$ (HOEAN), similarly to what has been found in longer alkyl chain ILs, such as alkyl-imidazolium ones. Such diffraction feature was pointed out as well by Greaves et al.,[28] who reported the SAXS and WAXS spectra of EAN up to 3 $Å^{-1}$, and by Umebayashi and co-workers[29] (spectrum up to 16 $Å^{-1}$). The highest relative intensity of this peak, among all diffraction experiments, is observed in the neutron diffraction patterns of the *N*-methyl deuterated compound ("d_3").

The presence of a low Q peak is presently considered as a direct experimental evidence of the heterogeneous microstructure of bulk ionic liquids, and is a largely debated topic (see, e.g., Russina et al.,[30−32] Hardacre et al.,[33] Castner et al.,[34] Fuji et al.,[35] Annapureddy et al.,[36] Fruchey et al.,[37] Kashyap et al.,[38] and Siqueira et al.[39])

In the cited paper by Hayes et al.,[24] the structural organization of EAN was described as a disordered L3-sponge phase, with small domain size. EAN was also the topic of a paper by Fumino et al.[40] who reported the low-frequency vibrational FTIR spectra of PAN, EAN and DMAN (dimethylammonium nitrate), and their description on the basis of DFT calculations. Their analysis indicates the existence of an extended, hydrogen bond-driven, three-dimensional network comparable to that of liquid water, although the larger ionic sizes and their donor–acceptor properties do not allow the formation of a tetrahedral network. The effect of the lower symmetry environment on spectroscopic properties was also discussed in a communication by Krüger et al.[41]

Concerning modeling results, apart from the empirical potential structure refinement (EPSR) approach derived by data fitting in the cited works,[24,25] Umebayashi et al.[29] interpreted the diffraction patterns using structure factors and radial distribution functions calculated from a classical molecular dynamics trajectory, using an *ad hoc* modified OPLS/AA force field; the study was extended to the upper homologues of EAN (PAN, propyl; BAN, butyl) in a recent study by the same group.[42] Their X-ray data description is overall good. Of particular interest to us in the present work is the evident fingerprint of the ionic couple interaction (mediated by H-bonds) that corresponds to a feature around 3.5 Å in the Diff(r) function (see Figure 2, bottom panel). This feature is reproduced by Umebayashi et al. model, but the average acceptor-proton (N–H...O) distances appears to be too large, compared with typical N–H–O H-bonding patterns (see refs 43 and 44).

One of the reason behind the present study is therefore that of trying an improvement of the OPLS force field in order to be able to (a) reproduce the X-ray diffraction pattern, (b) reliably describe the H-bonding feature, and (c) provide a local structural organization which is in better accordance with *ab initio* calculations (refs 43 and 44). Our approach stems from the evidence reported in our recent study, where a geometric structure of solid monomethylammonium nitrate (MMAN) was presented,[44] and in the Car–Parrinello MD studies by Zahn et al., that described the features of hydrogen bond contacts in liquid MMAN[43] and in its water solutions.[45]

In the present work, we shall also report new measurements of liquid EAN and HOEAN with our energy-dispersive X-ray diffractometer over a large Q range (0–20 $Å^{-1}$); as far as we know, a complete X-ray spectrum for HOEAN has not been recorded so far.

To interpret the diffraction patterns, we have calculated static structure factor and radial distribution curves from a series of new MD simulations, that were run employing both a two-body OPLS-based force field[46] and a force field obtained by adding a three-body term to the previous one. As we will show, the latter model is also able to satisfactorily reproduce many of the key characteristics of the neutron diffraction spectra reported (Figure 6 and ref 24) without the need of any additional parameter adjustment.

A general-purpose two-body force field such as OPLS turns out to be unable to describe satisfactorily all the experimental properties observed, with particular respect to the above-mentioned ionic pairing shown by X-ray measurements. One possible remedy for this situation is to "fit" a new set of force field parameters (for example the Lennard-Jones ones) in order

dx.doi.org/10.1021/jp306110g | *J. Phys. Chem. B* 2012, 116, 13024−13032

to provide a good comparison with better description of experimental data. Following this route has the obvious disadvantage of risking losing generality and transferability of the force field. Moreover, such fitted potential may present unphysical interactions terms which behave correctly in predicting the particular set of experimental data to which it was fitted, but may fail in providing an overall good description of other physical properties. This is the reason why we have attempted here a different route. We have maintained the generality of the OPLS force field (with very minor adjustments dictated by obvious physical considerations) and we have added a reasonable three-body term in order to model the H-bond interaction in the ionic couple. We shall show below, in fact, that the introduction of a three-body term centered on the acceptor-proton-donor triplets (N−H···O) remarkably improves the agreement with experimental data in the relevant Q range, thereby suggesting that a simple two-body decomposition of the global force acting in the real system might be insufficient (see for example ref 47 for an example on the necessity of introducing three-body terms in the water potential description).

EXPERIMENTAL SECTION

EAN was purchased from Aldrich (>97% purity); HOEAN was synthesized according to the following procedure:

HNO_3 (65 wt %/wt, 11 mL, 0.16 mol) was cautiously added dropwise while stirring to a solution of ethanolamine (9.9 mL, 0.16 mol) in MeOH (10 mL), cooled at −10 °C. The reaction mixture was stirred for 1 h at the same temperature and after that time the solvent was removed under reduced pressure on a rotary evaporator. Data of ethanolammoniumnitrate (HOEAN): metastable white solid; 98% yield; d = 1.35 g·cm^{-3}. ^{1}H NMR (DMSO-d_6): 7.77 (bs, 3H), 5.11 (bs, 1H), 3.56 (t, J = 5.3, 2H), 2.86 (d, J = 5.3, 2H). ^{13}C NMR (DMSO-d_6): 57.6, 41.3.

Both compounds were dried by keeping them under high vacuum pump for 72 h while stirring. The water final content was evaluated by ^{1}H NMR analysis (H_2O < 0.003 wt %). The compounds were put into quartz capillaries just before the measurements.

X-RAY DIFFRACTION

The large angle X-ray scattering experiments were performed using the noncommercial energy-scanning diffractometer built in the Department of Chemistry at the University "La Sapienza" of Rome (Italian Patent No. 01126484—June 23, 1993). For a detailed description of instrument, technique, and the experimental protocol of the data acquisition phase, the reader is referred, to refs 48−52. In this experiment, the new 0−2ϑ instrument geometry (only one of the two diffractometer arms can move) was used; the samples were put in 2-mm quartz cylindrical capillaries. In such setup, higher diffracted intensities can be recorded. The appropriate measuring time (i.e., number of counts) was chosen to obtain scattering variable (Q) spectra with high signal-to-noise ratio (600 000 counts on average). The diffraction patterns acquired at the different angles were then joined to obtain a continuous spectrum in Q.[53] Only five diffraction angles are enough to cover a Q-spectrum ranging from 0.1 to 19.56 Å^{-1}.

The total intensity of the radiation scattered by a sample in a diffraction experiment, after the correction for systematic effects (polarization, absorption, incoherent and multiple scattering) and rescaling to absolute units (electron units per stochiometric unit), can be expressed as the sum of two terms:[54]

$$I_{\exp}(Q)_{E.U} = \sum_{i=1}^{N} x_i f_i^2 + I(Q) \tag{1}$$

The first term represents the independent atomic scattering from the atoms in a stochiometric unit, while $I(Q)$ is the "total (static) structure factor" and constitutes the structurally sensitive part of the scattering intensity, being due to the interference contributions from different atoms.

The variable Q is the magnitude of the transferred momentum, and depends on the scattering angle (2ϑ), according to the relation $Q = 4\pi(\sin\vartheta/\lambda)$, which is equal to $Q \approx 1.0136 \sin\vartheta$, if E is expressed in keV and Q in Å^{-1}. The function $I(Q)$ is related to the pair correlation functions descriptive of the structure, according to the formula

$$I(Q) = \sum_{i=1}^{N}\sum_{j=1}^{N} x_i x_j f_i f_j H_{ij}(Q) \tag{2}$$

where we have introduced the partial structure functions H_{ij} defined in terms of pair correlation functions by the Fourier integral[55]

$$H_{ij}(Q) = 4\pi\rho_0 \int_0^\infty r^2(g_{ij}(r) - 1)\frac{\sin(Qr)}{Qr}\,dr \tag{3}$$

(ρ_0 is the bulk number density of the system, x_i are the numerical concentrations of the species and f_i their Q-dependent X-ray scattering factors).

By inverting this Fourier transform, we get

$$g_{ij}(r) = 1 + \frac{1}{2\pi^2 r\rho_0}\int_0^\infty QH_{ij}(Q)\sin(rQ)\,dQ \tag{4}$$

Therefore, the link between experimental data and molecular modeling is particularly important, considering the fact that the quantity obtainable from a single X-ray diffraction experiment is a linear combination of H_{ij} and that the deconvolution into its components is not directly feasible. The structure functions, both the one derived from experimental diffraction patterns and that obtained from theoretical pair correlation functions were multiplied by a modification function $M(Q)$, a sharpening factor, necessary to improve the curve resolution at high Q, and then Fourier-transformed into a modified (total) correlation function $G(r)$ or a radial distribution function ($D(r)$), according to the relation[56,57]

$$D(r) - 4\pi r^2\rho_0 = (G(r) - 1) = \frac{2r}{\pi}\int_0^\infty QI(Q)\sin(rQ)M(Q)\,dQ \tag{5}$$

If the uniform distribution component is dropped (which corresponds to the second term of the subtraction, or to 1), we obtain the differential correlation function Diff(r), containing only the structural contribution to the distribution function. For a comprehensive report of all the formulas, see.[56,57] Summarizing, the comparison between experimental and model data will be carried out using both $QI(Q)M(Q)$ ("reciprocal space") and Diff(r) ("direct space"), while for the discussion of the model characteristics we will use both g_{ij} (r) and Diff(r), which share the same information, but emphasize differently the details, since $g(r)$ is more resolved for low range and Diff(r) for medium-long-range distances (outer shells).

dx.doi.org/10.1021/jp306110g | J. Phys. Chem. B 2012, 116, 13024−13032

Several studies demonstrating the validity of this experimental-computational approach have been published so far (see, e.g., refs 58−63); all the functions were calculated using in-house written codes.

The structure factors (Figure 1 and Figure 3, upper panel) show the broad peaks typically found in liquids, with a moderate degree of ordering suggested by the intensity of the peaks. Although peak assignments in reciprocal space is not directly feasible, since many interference patterns from the various scattering centers contribute to each peak, we can state that the intramolecular scattering is responsible for almost all the observed intensity beyond 2 Å^{-1}, while intermolecular contacts originate the "principal peak" falling at about 1.70 Å^{-1}. If the experimental radial distribution function is considered (Figure 1 and Figure 3, middle/lower panel), after the two sharp molecular peaks, falling at 1.3 and 2.15 Å, that are attributed to atom directly bonded and 1−3 contacts, there is an intense peak at 3.5 Å, that is considered as a fingerprint of the ionic couple (see modeling section); four intermolecular "shells" with maxima at 4.85, 8.30, 12.20, and 15.75 Å are found beyond. The spatial correlation of the system decays rapidly after 17 Å, and the signal becomes buried into the noise.

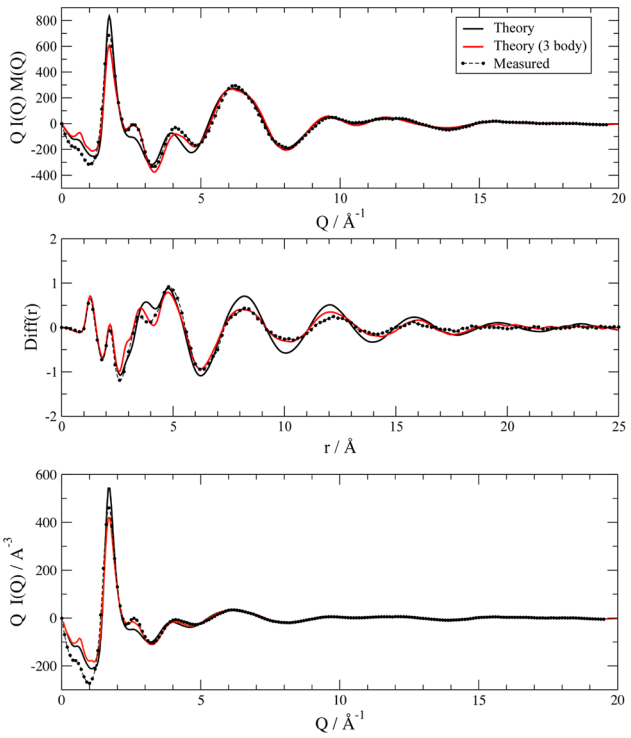

Figure 1. Upper panel: EAN $Q{\cdot}I(Q)M(Q)$·experiments and theory. Middle panel: Fourier transform of the above data, Diff(r) from experiment. Lower panel: same as in upper panel, but without sharpening factor.

NEUTRON DIFFRACTION

Neutron scattering measurements of EAN (all ^{1}H) were conducted at the DNS beamline at the FRM-II reactor in Garching, Germany. The incident neutron wavelength of 4.74 Å has been selected by a 30 double focusing PG[002] monochromator from a white beam in the neutron guide NL6, and results in a Q-range up to 2.4 Å^{-1}. The coherent and incoherent contributions in the scattered intensity were separated via polarization analysis in a wide scattering angle range of $0° < 2\vartheta < 120°$.

Theoretical structure factors were calculated using the same formulas 2 and 3 reported in the above description for X-rays, where the X-ray scattering factors f were replaced with the neutron scattering length b;[64] data were normalized by the total-scattering cross section $\sum x_i b_i^2$ to obtain a $S(Q)$ function[56] (Figure 5 and 6).

THEORETICAL METHODS

Molecular dynamics (MD) simulations have been performed using the DLPOLY 4 code.[65] For HOEAN we have used a cell made of 1000 ionic couples that were equilibrated for 3 ns in an isothermic-isobaric ensemble (*NPT*). The very small fraction of neutral compounds present at equilibrium in the neat liquid (about 10^{-5} mol dm^{-3}, see the introduction) was omitted in our model. Production for the structural observables and features has followed for another 2 ns in the canonical ensemble (*NVT*). For EAN, we used the same strategy with a slightly larger cell containing 2500 ionic couples in order to properly include long-range correlations on a length-scale of about 10−15 Å, whose existence emerged on the basis of low Q diffraction data from Atkin et al.[23] Dynamics was performed by means of a leapfrog-Verlet scheme with integration step of 1 fs. Only C−H distances were constrained at 1.09 Å with the SHAKE algorithm, while all other structural motifs were completely flexible. Particle mesh Ewald was used for the calculation of electrostatic interactions for distances larger than 12 Å, which is also the cutoff for the van der Waals interactions. HOEAN can be a metastable liquid at room temperature,[11,66] therefore the equilibration and production temperature chosen was 350 K in order to avoid artificially "freezing" the simulated system in a glassy state.

The atomic types used are reported in Chart 1. The naming conventions, when possible, are those of the OPLS force field.

The interaction potentials (the force field) adopted here is essentially an OPLS force field.[46,67] This force fields family is suited to achieve a good and reliable representation of the structure in organic molecular liquids and has been built and tested in this respect. However, in the case of ionic liquids, the very large energetic contributions due to the net charges of the constituents makes the OPLS parametrization weaker, especially in providing a correct description of density which turns out to be invariably and significantly larger that the experimental one. One way to deal with such effect is to change the Lennard-Jones (LJ) parameters in order to obtain the expected density. For example, in refs 24, 29, and 35, the LJ parameters of the acidic hydrogens in the NH_3^+ group (or in the OH one) have been chosen to have the same value of the aliphatic H atoms. This, in our opinion, creates an excluded volume within the ionic couples that essentially makes densities fit more nicely to experiments. Such choice, however, might provide an unphysical description of the local geometry of the H-bonding features, since it assumes that the acidic hydrogen atoms have the same electronic densities as the aliphatic ones, which is rather incorrect when the heteropolarity of the bond is relevant (N−H, O−H, etc.). The force field we adopt, as we have said above, is essentially OPLS with few modifications:

LJ parameters of the nitrate anion have been taken from[68] where a specific set of parameters was obtained by fitting structural data from MD simulations to the crystalline phases of ammonium nitrate; LJ parameters on the acidic protons are set to ε = 0.1 kcal/mol and σ = 0.8 Å. This choice is in line with

dx.doi.org/10.1021/jp306110g | J. Phys. Chem. B 2012, 116, 13024−13032

the original OPLS force field,[46,67] where LJ parameters are set to zero for these atoms. The charges on the two molecular components of the ionic couple have been determined by fitting the MP2 electronic density from a single point calculation at the MP2/6-311+G(d,p) level. The force field calculations have been performed using a dielectric constant in order to scale the electrostatic charges to 0.8 of their values. This is in agreement with the amount of charge transfer that can be noticed by performing DFT optimization on small clusters of the systems.[69] For example, a cluster made of 6 ionic couples optimized at the B3LYP/6-311+G (d,p) level of theory provides a nitrate total charge (when fitted to its electrostatic potential obtained by the SCF/DFT electronic density) that on average is equal to −0.73e. This proves that there is a substantial amount of charge transfer and polarization in these systems that can justify the use of scaled charges as we have done in the present calculations.

With these parameters (without the three body term) the density of the two fluids turns out to be 1.20 g·cm^{-3} at room temperature for EAN (1.216 is the measured value from ref 66) and 1.32 g·cm^{-3} for HOEAN (1.265 in ref 66, but we found 1.34 g·cm^{-3} with our own volumetric measurement which is in line with 1.39 reported by ref 70). It is to be noticed that HOEAN is a supercooled liquid at room temperature and therefore measurements might depend on the metastable physical state of the sample. We shall report below the results obtained with the above force field (two-body only) and those obtained with the addition of a three-body term centered on the N_3-H_3-ON triplets which has the form:

$$U = D_{hb}\cos^4(\vartheta_{jik})[5(R_{hb}/r_{jk})^{12} - 6(R_{hb}/r_{jk})^{10}] \quad (6)$$

We have used various combinations of strength and equilibrium distance, but the results are almost insensitive to reasonable changes of the two parameters. Our final choice was D_{hb} = 10 or 15 kJ and R_{hb} = 2.8 Å. The three-body term is active only when the three atoms are within 5 Å from each other. The addition of the three-body term increases the density of the simulated liquids of about 2% with D_{hb} = 10 kJ and 4% for D_{hb} = 15 kJ. In our simulations, we have preferred to keep the system under the *NVT* thermostat using the volumes predetermined with the 2-body force field. Two further control calculations to assess the performance of the 3B term were carried out (EAN only):

(1) A 1 ns trajectory without the 3B term was generated, starting from the final structure of the 3B trajectory. In doing so, we could verify that no special bias had been introduced by the 3B term, since after about 200 ps, the patterns obtained without 3B (Figure 1 and 2) could be recovered;

(2) A complete simulation (1 ns equilibration +1 ns production) using the "large" H3 LJ parameters of ref 24 (or refs 29 and 35) and the three-body term described above was accomplished. In this case, we obtained a good fit of experimental X-ray functions quite similar to those shown in Figure 1 and 2, while the ON−H3 $g(r)$'s were shifted significantly toward larger distances (2.4 Å), if compared with those obtained *ab initio* in ref 43 and in this work (Figure 2 lower panel). All the force fields used in this study are reported in the Supporting Information.

RESULTS AND DISCUSSION

The first result we present is a comparison of the structure factor calculated for our two models (with and without three-body term) and the corresponding experimental measurements for the EAN compound. In Figure 1 we report the $Q{\cdot}I(Q)$ $M(Q)$ in the upper panel, while in the middle one, we plot the Diff(r) functions obtained by Fourier transformation (eq 5) of the same data; $I(Q)$ without sharpening is reported in the lower panel to allow a comparison with literature data. In the two-body case, we have a decent agreement on all range of distance except in the intermediate range where we have only a qualitative agreement. From the inspection of the Diff(r) function we notice that simulations overestimate the signal at long-range (although we correctly predict four solvation shells) and only partially account for the feature centered around 3.5 Å that is thought to be a direct manifestation of the ionic couple correlation (i.e., nitrate−ammonium). On the whole, our results look very similar to those presented in ref 42.

We propose to improve the data description by adding a three-body potential term (3B) leading to a weakly binding among the H3, the N3, and the ON atoms. The advantage of such interaction potential is 2-fold: it is weak, and it does not bind indefinitely the ionic couples, therefore leaving them the possibility of dissociating during the simulation and it represents a source of additional disorder in the model since it should mimic the hydrogen-bonding feature of these systems, which is characterized by a partial saturation of the acceptor−donor network. Experimental[44] and theoretical[43] evidence suggest, in fact, that two of the three possible hydrogen bonds are stronger than the other.

As can be clearly seen (Figure 1−5), the introduction of the three-body term greatly improves the agreement with experimental data under many points of view. In the structure factor, the intermediate range (2−5 Å^{-1}) is now in excellent agreement with experimental data, and this generates a Diff(r), which now correctly shows the peak at 3.5 Å. Furthermore, the overestimated long-range shell structure noticed in the two-body model disappears when using the three-body term. This last effect clearly points out how the presence of an asymmetric H-bond feature (actually induced in our simulation by the introduction of the three-body term) is one of the sources of structural disorder that is responsible for the liquid state of these compounds, even in mild conditions.

In Figure 2 we report the radial distribution functions obtained from both models that are relevant for a description of the H-bonding feature. We notice the following:

- The average distance between the acceptor (ON) and the donor (N3) is 3 Å in perfect agreement with what has already been reported in ref 43 and by us for the solid MAN compound.[44] A second shell contact is clearly visible around 4.6−4.9 Å.
- The distance between the acidic H and the acceptor is small, around 1.9−2.0 Å in agreement with what we had found for the MAN compound[44] and with what has been found by Kirchner and co-workers[43,45] by *ab initio* MD in the MAN compound. It is remarkable that the shape of the present radial distribution functions is very similar to those obtained with Car−Parrinello first principles MD on the analogous compound MAN.
- The present data are compatible with *ab initio* minimization (see ref 44 for further details) of isolated small cluster of EAN ionic couples. In Figure 2 we also

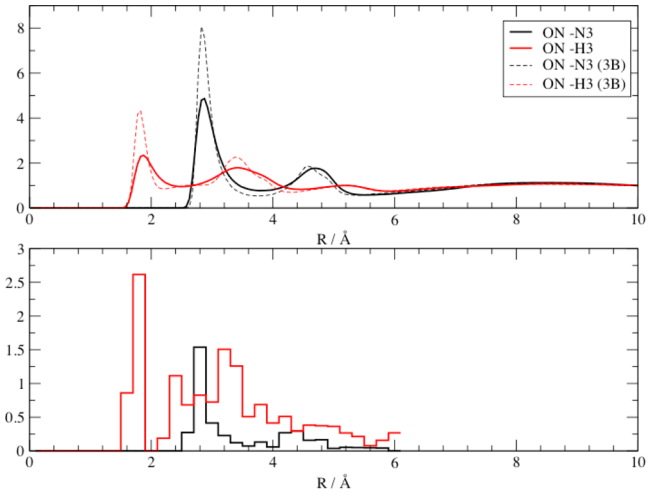

Figure 2. Upper panel: EAN radial distribution functions for the atoms involved in the H-bond. Lower panel: histogram of the H-bond distances occurring in a *ab initio*/DFT minimization of a EAN cluster of eight ionic couples.

report an histogram of the occurrence of the same distances in a rather large cluster of 8 ionic couples obtained by a minimization procedure which ended up yielding a stationary point structure at the ωB97XD/6-31+G(d) level. These calculations, which include dispersion contributions in the range separated functional ωB97X, are considered the "state-of-the-art" of density functional theory, and have proven to accurately reproduce well weak interactions such as hydrogen bonds and van der Waals forces.[71] All QM calculations were performed with Gaussian 09.[72]

Analogous results for HOEAN are reported in Figure 3 and Figure 4. The discrepancies between experiments and theory

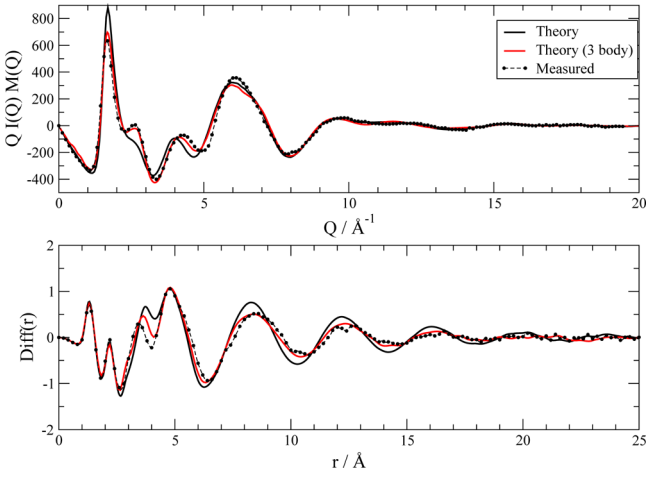

Figure 3. Upper panel: HOEAN $Q{\cdot}I(Q)$·experiments and theory. Lower panel: Fourier transform of the above data, Diff(r) from experiments and theory.

(2-body) are evident for HOEAN as well. The intermediate range of both the structure factor and of the radial distribution shows only a qualitative agreement with experiment. In particular the radial peak at 3.5 Å seems to be reproduced rather inaccurately by the model. In the MD model, this peak is in fact located at 3.9 Å thereby positioning the cation−anion

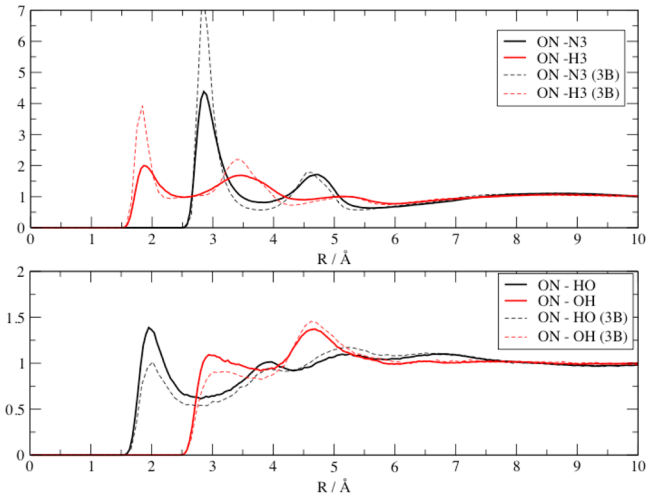

Figure 4. Upper panel: HOEAN radial distribution functions for the atoms involved in the H-bond.

average distance at too large values, since this peak arises mainly because of the anion−cation spatial correlation.

With the three-body potential, also in HOEAN, the agreement with experiments is very good in all the distance range and the cation−anion peak is now better reproduced by our calculations. An additional effect of the 3B term is that of creating a less structured Diff(r) for both compounds, which is more similar to the experimental pattern.

A general consequence, though a rather obvious one, is that the radial contacts between the H-bond forming atoms are enhanced.

A further assessment of the goodness of our model is reported in Figure 5 and 6 where we show the neutron

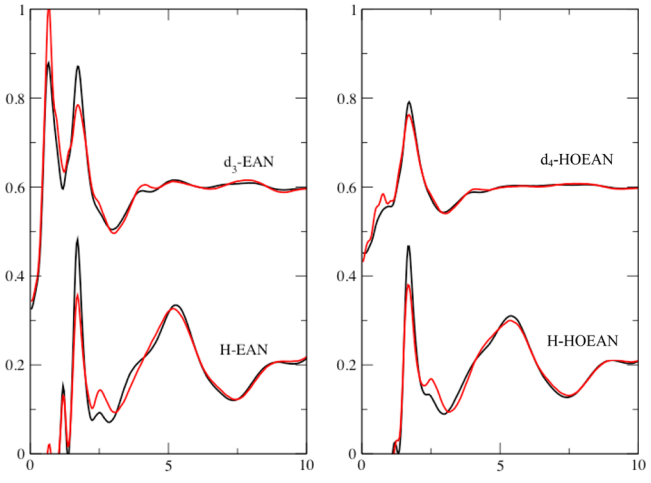

Figure 5. Predicted neutron scattering $S(Q)$ from our model. Black lines: OPLS model. Red lines: OPLS + three-body. The deuteration model is indicated in the figure. H-EAN and H-HOEAN are fully protiated while d_3 and d_4 are compounds with deuteration at the acidic hydrogens (non aliphatic).

diffraction pattern obtained by our simulations by substituting, where necessary, the scattering factors of H with those of D. Qualitatively, our results closely resemble those reported by Hayes and co-workers in ref 24. The partially deuterated samples (d_3-EAN and d_4-HOEAN where the acidic protons are substituted) clearly show the presence of a prepeak that is

dx.doi.org/10.1021/jp306110g | J. Phys. Chem. B 2012, 116, 13024−13032

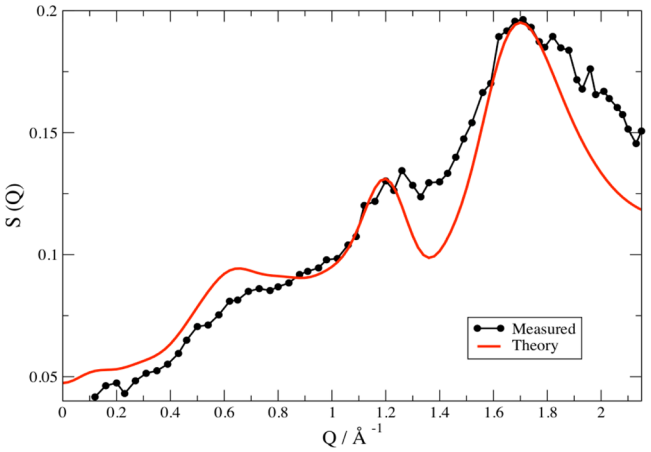

Figure 6. Protiated EAN neutron scattering: experiments and theory. Symbols: experimental neutron scattering intensities. Lines: model.

particularly enhanced in the EAN case. If we separate the atomic pair contributions to the X-ray $I(Q)$, we can easily see that the main contribution to the prepeak are the HC3 hydrogen atoms, i.e., the aliphatic chain ones as noticed in other system.

This feature can be pointed out in our neutron data for all-protiated EAN as well (Figure 6). This prepeak is extremely important because it shows the formation of heterogeneous structures on a 10-Å scale.

As pointed out by Hayes et al.[24] and discussed by Russina et al.,[30,31] the presence of the OH terminal group tends to destroy such correlations and therefore also the underlying structures that produce it. This effect is correctly and naturally provided by our model potential. It is also worth stressing that the H-bonding feature of the O−H---ON connection seems only slightly weaker than the N−H---ON counterpart (see the radial distribution reported in Figure 4), although only one possible donor exists for the former H-bond. The strength of this O−H---ON H-bond is therefore sufficient to break the apolar−polar domain separations which are thought to be the main driving force for the formation of the nanoheterogeneities causing the prepeak to appear in EAN. Another interesting feature of neutron data (Figure 6) is the evident peak falling at 1.2 $Å^{-1}$. Such peak clearly distinguishes the neutron pattern from the X-ray one, where there is only one principal peak falling at 1.7 $Å^{-1}$. From the analysis of the individual contributions (partial scattering factors weighted by scattering lengths, eq 2 and 3), the most important contributions to the 1.2 $Å^{-1}$ peak originate from C3−N3 (cation−cation), HC/HC3/H3-NN (cation−anion) and NN-NN (anion−anion) correlations; explicative pictures and further explanation are reported as Supporting Information.

Three-dimensional densities around the cation and anion are displayed in Figure 7. In the left panel we describe the cation surroundings: we have reported the NO_3^- center of mass (largely coincident with the N atom) in red and the cation center of mass density in orange (transparent).

The distribution of the first shell of anions is rather regular and we can notice that each H3 points to a nitrate ion distribution (this is consistent with ref 24) and that the angle of the specific N3−H3−ON is rather variable giving rise to a broad distribution. The cation−cation first solvation shell has a more complex pattern: most of the cation centers of mass are

Figure 7. EAN: three-dimensional spatial distribution functions for the cation (left) and anion (right) surroundings. See text for details.

located in the direction of the C−N bond and around the alkyl tail of the EA^+ cation.

In the right panel we report the distributions around the NO_3^- ion: in gray the relative positioning of the EA^+ centers of mass are shown (again in agreement with refs 24 and 43). In yellow (transparent), we have reported the distribution of the H3 atoms around NO_3 anion: we see that its shape is not defined, thus confirming that distribution of H-bond values is rather broad in agreement with the findings reported in ref 43. The green distribution in Figure 7 is the anion−anion distribution. On the whole, we can say that the new model potential presented here accounts correctly for all the various features that have been pointed out by the experimental measurements. However, it must be stressed that, for the moment, we have limited our analysis to the static structural properties.

■ CONCLUSIONS AND PERSPECTIVES

In this work, we have reported a comparison between experimental X-ray scattering profiles and MD simulations for two prototypical protic ionic liquids: EAN and HOEAN. The agreement we have obtained is remarkably good and has allowed us to trace precise structural features of the local liquid structure. These liquids, as many other ionic liquids, are organized in a disordered three-dimensional ionic network that sees, locally, an alternation between ions of opposite signs.

The disorder in such liquids is the result of many effects: on one side we find the interplay between the strong charge−charge interaction which tend to make the system solid and the "hydrophobic" interactions due to the alkyl chains that induce aggregation phenomena that locally weaken the cohesive energy. On the other side, the asymmetric molecular geometry of the cation is also an important source of structural disorder (MAN, which has a smaller alkyl chain, is solid even well above room temperature, despite the fact that the electrostatic interaction would certainly be very similar to the one in EAN). Finally, an additional source of disorder in these liquids is the presence of H-bonds: as already suggested in earlier works (see Fumino et al.[73]) these directional H-bonds represent a source of defects in the Coulombic network leading to more disordered ionic liquids. The presence of H-bonds in protic ionic liquids may lead to more disordered system that is the opposite of what can be expected by looking at the behavior of typical molecular liquids. From the computational point of view, we have shown above that a two-body only force field tends to overestimate the long-range order in the present compounds. We have also shown how, by switching on the three-body term, the fluid becomes less structured, thereby making the radial distribution profile at long-range more similar to the experimental one, and therefore

dx.doi.org/10.1021/jp306110g | J. Phys. Chem. B 2012, 116, 13024−13032

confirming that the inclusion of an attractive H-bond-like bonding term can actually increase disorder.

More generally, we have shown with our calculations how the introduction of a three-body term makes the simulation able to grasp the short- and long-range structure with remarkable precision in a very natural way. Although we are aware that it may be possible to find a set of parameters for the two-body force field able to reproduce a particular experimental pattern, we believe that our study not only reproduces the experimental data satisfactorily, but actually sheds some new light on the rather complex molecular interactions at play in the compounds studied. The remarkable improvement of the agreement with the experimental observables obtained upon switching on the three-body term does tell us something on how complex the real interaction network in these systems actually is and on the importance that many-body effects definitely have in governing their behavior.

■ ASSOCIATED CONTENT

Supporting Information

Complete force field used in the calculations (DL_POLY Format) and plots of the positive (Figure 1S) and negative (Figure 2S) contributions to the distinctive 1.2 $Å^{-1}$ peak of the neutron structure factor of EAN. This material is available free of charge via the Internet at http://pubs.acs.org.

■ AUTHOR INFORMATION

Corresponding Author

*E-mail: (L.G.) l.gontrani@caspur.it; (E.B.) e.bodo@caspur.it.

Notes

The authors declare no competing financial interest.

■ ACKNOWLEDGMENTS

This work was supported from CASPUR (Centro di Applicazione di Supercalcolo per Universita′ e Ricerca, Rome Supercomputing Center, Grant std11-465 and std12-011), from CINECA (IscrA_ASIL), and from the Scientific Committee of the University of Rome. A.T. wishes to thank Dr. Y. Su and Dr. W. Borghols for their skillful support in performing the experiment at DNS and acknowledges the access to the DNS spectrometer. This research project has been supported by the European Commission under the seventh Framework Programme through the "Research Infrastructures" action of the "Capacities" Programme, NMI3-II Grant No. 283883. L.G. and A.T. acknowledge support from FIRB (RBFR086BOQ) and PRIN (2009WHPHRH).

■ REFERENCES

(1) Zhu, S.; Wu, Y.; Chen, Q.; Yu, Z.; Wang, C.; Jin, S.; Ding, Y.; Wu, G. *Green Chem.* **2006**, *8*, 325.
(2) Wang, H.; Gurau, G.; Rogers, R. D. *Chem. Soc. Rev.* **2012**, *41* (4), 1519.
(3) Bradley, A. E.; Hatter, J. E.; Nieuwenhuyzen, M.; Pitner, W. R.; Seddon, K. R.; Thied, R. C. *Inorg. Chem.* **2002**, *41*, 1692.
(4) Baston, G. M. N.; Bradley, A. E.; Gorman, T.; Hamblett, I.; Hardacre, C.; Hatter, J. E.; Healy, M. J. F.; Hodgson, B.; Lewin, R.; Lovell, K. V.; Newton, G. W. A.; Nieuwenhuyzen, M.; Pitner, W. R.; Rooney, D. W.; Sanders, D.; Seddon, K. R.; Simms, H. E.; Thied, R. C. Ionic liquids for the nuclear industry: A radiochemical, structural, and electrochemical investigation. In *Ionic Liquids: Industrial Applications for Green Chemistry*; Rogers, R. D., Seddon, K. R., Eds.; American Chemical Society: Washington DC, 2002; Vol. *818*, pp 162−177.
(5) Gan, Q.; Rooney, D.; Xue, M.; Thompson, G.; Zou, Y. *J. Membr. Sci.* **2006**, *280*, 948.
(6) Lovelock, K. R. *Phys. Chem. Chem. Phys.* **2012**, *14* (15), 5071.
(7) Brennecke, J. F.; Gurkan, B. E. *J. Phys. Chem. Lett.* **2010**, *1* (24), 3459.
(8) D'Angelo, P.; Zitolo, A.; Migliorati, V.; Bodo, E.; Aquilanti, G.; Hazemann, J.-L.; Testemale, D.; Mancini, G.; Caminiti, R. *J. Chem. Phys.* **2011**, *135*, 074505.
(9) Walden, P. *Bull. Acad. Imper. Sci. St. Pétersbourg* **1914**, *8*, 405.
(10) Gabriel, S.; Weiner, J. *Ber. Dtsch. Chem. Ges.* **1888**, *21*, 2669.
(11) Belieres, J. P.; Angell, C. A. *J. Phys. Chem. B* **2007**, *111*, 4926.
(12) MacFarlane, D. R.; Seddon, K. R. *Aust. J. Chem.* **2007**, *60*, 3−5.
(13) Kanzaki, R.; Uchida, K.; Song, X.; Umebayashi, Y.; Ishiguro, S. *Anal. Sci.* **2008**, *24* (10), 1347−1349.
(14) Yoshizawa, M.; Xu, W.; Angell, C. A. *J. Am. Chem. Soc.* **2003**, *125* (50), 15411.
(15) Garlitz, J. A.; Summers, C. A.; Flowers, R. A., II; Borgstahl, G. E. O. *Acta Crystallogr.* **1999**, *D55*, 2037.
(16) Shotwell, J. B.; Flowers, R. A. *Electroanalysis* **2000**, *12* (3), 223.
(17) Xu, W.; Angell, C. A. *Science* **2003**, *302*, 422.
(18) Greaves, T. L.; Drummond, C. J. *Chem. Soc. Rev.* **2008**, *37*, 1709.
(19) Picquet, M.; Tkatchenko, I.; Tommasi, I.; Wasserscheid, P.; Zimmermann, J. *Adv. Synth. Catal.* **2003**, *345*, 959.
(20) U.S. Patent 6001197 http://www.freepatentsonline.com/6001197.html
(21) Volk, F.; Bathelt, H. *Prop. Explos., Pyrotech.* **2002**, *27*, 136.
(22) Summers, C. A.; Flowers, R. A., 2nd *Protein Sci.* **2000**, *9* (10), 2001.
(23) Atkin, R.; Warr, G. G. *J. Phys. Chem. B* **2008**, *112* (14), 4164.
(24) Hayes, R.; Imberti, S.; Warr, G. G.; Atkin, R. *Phys. Chem. Chem. Phys.* **2011**, *13*, 3237.
(25) Hayes, R.; Imberti., S.; Warr, G. G.; Atkin, R. *Phys. Chem. Chem. Phys.* **2011**, *13*, 13544.
(26) Greaves, T. L.; Weerawardena, A.; Fong, C.; Drummond, C. J. *J. Phys. Chem. B* **2007**, *111* (16), 4082.
(27) Greaves, T. L.; Weerawardena, A.; Krodkiewska, I.; Drummond, C. J. *J. Phys. Chem. B* **2008**, *112* (3), 896−905.
(28) Greaves, T. L.; Kennedy, D. F.; Mudie, S. T.; Drummond, C. J. *J. Phys. Chem. B* **2010**, *114*, 10022.
(29) Umebayashi, Y.; Chung, W.; Mitsugi, T.; Fukuda, S.; Takeuchi, M.; Fuji, K.; Takamuku, T.; Kanzaki, R.; Ishiguro, S. *J. Comput. Chem. Jpn.* **2008**, *7* (4), 125.
(30) Russina, O.; Triolo, A. *Faraday Discuss.* **2012**, *154*, 97.
(31) Russina, O.; Triolo, A.; Gontrani, L.; Caminiti, R. *J. Phys. Chem. Lett.* **2012**, *3* (1), 27.
(32) Triolo, A.; Russina, O.; Bleif, H.-J.; Di Cola, E. *J. Phys. Chem. B* **2007**, *111*, 4641.
(33) Hardacre, C.; Holbrey, J. D.; Mullan, C. L.; Youngs, T. G. A.; Bowron, D. T. *J. Chem. Phys.* **2010**, *133*, 074510.
(34) Castner, E. W. J.; Margulis, C. J.; Maroncelli, M.; Wishart, J. F. *Annu. Rev. Phys. Chem.* **2011**, *62*, 85.
(35) Fujii, K.; Kanzaki, R.; Takamuku, T.; Kameda, Y.; Kohara, S.; Kanakubo, M.; Shibayama, M.; Ishiguro, S.; Umebayashi, Y. *J. Chem. Phys.* **2011**, *35*, 244502.
(36) Annapureddy, H. V. R.; Kashyap, H. K.; De Biase, P. M.; Margulis, C. J. *J. Phys. Chem. B, 114* **2010**, *114*, 16838−16846.
(37) Fruchey, K.; Lawler, C. M.; Fayer, M. D. *J. Phys. Chem. B* **2012**, *116* (10), 3054−3064.
(38) Kashyap, H. K.; Santos, C. S.; Annapureddy, H. V. R.; Murthy, N. S.; Margulis, C. J.; Castner, E. W. J. *Faraday Discuss.* **2012**, *154*, 133−143.
(39) Siqueira, L. J. A.; Ribeiro, M. C. C. *J. Chem. Phys.* **2011**, *135*, 204506.
(40) Fumino, K.; Wulf, A.; Ludwig, R. *Angew. Chem., Int. Ed.* **2009**, *48*, 3184.
(41) Krüger, M.; Bründermann, E.; Funkner, S.; Weingärtner, H.; Havenith, M. *J. Chem. Phys.* **2010**, *132*, 101101.
(42) Song, X.; Hamano, H.; Minofar, B.; Kanzaki, R.; Fujii, K.; Kameda, Y.; Kohara, S.; Watanabe, M.; Ishiguro, S.; Umebayashi, Y. *J. Phys. Chem. B* **2012**, *116*, 2801.
(43) Zahn, S.; Thar, J.; Kirchner, B. *J. Chem. Phys.* **2010**, *132*, 124506.

(44) Bodo, E.; Postorino, P.; Mangialardo, S.; Piacente, G.; Ramondo, F.; Bosi, F.; Ballirano, P.; Caminiti, R. *J. Phys. Chem. B* **2011**, *115* (45), 13149.
(45) Zahn, S.; Wendler, K.; Delle Site, L.; Kirchner, B. *Phys. Chem. Chem. Phys.* **2011**, *13*, 1503.
(46) Kaminski, G. A.; Friesner, R. A.; Tirado-Rives, J.; Jorgensen, W. L. *J. Phys. Chem. B* **2001**, *105*, 6474.
(47) Bukowski, R.; Szalewicz, K.; Groenenboom, G. C.; van der Avoird, A. *Science* **2007**, *315*, 1249.
(48) Carbone, M.; Caminiti, R.; Sadun, C. *J. Mater. Chem.* **1996**, *6* (10), 1709.
(49) Rossi Albertini, V.; Bencivenni, L.; Caminiti, R.; Cilloco, F.; Sadun, C. *J. Macromol. Sci., Phys.* **1996**, *B35* (2), 199.
(50) Ballirano, P.; Caminiti, R.; Ercolani, C.; Maras, A.; Orrù, A. *J. Am. Chem. Soc.* **1998**, *120* (49), 12798.
(51) Atzei, D.; Ferri, T.; Sadun, C.; Sangiorgio, P.; Caminiti, R. *J. Am. Chem. Soc.* **2001**, *123* (11), 2552.
(52) Webpage http://webcaminiti.chem.uniroma1.it and references cited therein
(53) Murata, Y.; Nishikawa, K. *Bull. Chem. Soc. Jpn.* **1978**, *51*, 411.
(54) Plug, H. P.; Alexander, L. E. *X-Ray Diffraction Proceedings for Poly Crystalline and Amorphous Materials*, 2nd ed.; John Wiley and Sons: New York-London, 1974; p 79
(55) Pings, C. J.; Waser, J. *J. Chem. Phys.* **1968**, *48*, 3016.
(56) Keen, D. A. *J. Appl. Crystallogr.* **2001**, *34*, 172.
(57) Caminiti, R.; Licheri, G.; Piccaluga, G.; Pinna, G. *Rev. Inorg. Chem* **1979**, *1*, 333.
(58) Gontrani, L.; Ramondo, F.; Caminiti, R. *Chem. Phys. Lett.* **2006**, *417* (1−3), 200.
(59) Gontrani, L.; Russina, O.; Marincola, F. C.; Caminiti, R. *J. Chem. Phys.* **2009**, *131* (24), 244503.
(60) Bodo, E.; Gontrani, L.; Caminiti, R.; Plechkova, N. V.; Seddon, K. R.; Triolo. *J Phys. Chem. B* **2010**, *114* (49), 16398.
(61) Migliorati, V.; Ballirano, P.; Gontrani, L.; Triolo, A.; Caminiti, R. *J. Phys. Chem. B* **2011**, *115*, 4887.
(62) Migliorati, V.; Ballirano, P.; Gontrani, L.; Russina, O.; Caminiti, R. *J. Phys. Chem. B* **2011**, *115*, 11805.
(63) Migliorati, V.; Ballirano, P.; Gontrani, L.; Triolo, A.; Caminiti, R. *J. Phys. Chem. B* **2012**, *116*, 2104.
(64) http://www.ncnr.nist.gov/resources/n-lengths
(65) Todorov, I.; Smith, W.; Trachenko, K.; Dove, M. *J. Mater. Chem.* **2006**, *16*, 1611.
(66) Greaves, T. L.; Weerawardena, A.; Fong, C.; Krodkiewska, I.; Drummond, C. J. *J. Phys. Chem. B* **2006**, *110*, 22479.
(67) Jorgensen, W. L.; Maxwell, D. S.; Tirado-Rives, J. *J. Am. Chem. Soc.* **1996**, *118*, 11225.
(68) Sorescu, D. C.; Thompson, D. L. *J. Phys. Chem. A* **2001**, *105*, 720.
(69) (a) Bodo, E.; Chiricotto, M.; Caminiti, R. *J. Phys. Chem. B* **2011**, *115*, 14341. (b) Bodo, E.; Caminiti, R. Manuscript in preparation
(70) Belieres, J. P.; Angell, C. A. *J. Phys. Chem. B* **2007**, *111*, 4926.
(71) Chai, J. D.; Head-Gordon, M. *Phys. Chem. Chem. Phys.* **2008**, *10*, 6615.
(72) *Gaussian 09, Revision A.1*; Frisch, M. J.; Trucks, G. W.; Schlegel, H. B.; Scuseria, G. E.; Robb, M. A.; Cheeseman, J. R.; Scalmani, G.; Barone, V.; Mennucci, B.; Petersson, G. A.; Nakatsuji, H.; Caricato, M.; Li, X.; Hratchian, H. P.; Izmaylov, A. F.; Bloino, J.; Zheng, G.; Sonnenberg, J. L.; Hada, M.; Ehara, M.; Toyota, K.; Fukuda, R.; Hasegawa, J.; Ishida, M.; Nakajima, T.; Honda, Y.; Kitao, O.; Nakai, H.; Vreven, T.; Montgomery, Jr., J. A.; Peralta, J. E.; Ogliaro, F.; Bearpark, M.; Heyd, J. J.; Brothers, E.; Kudin, K. N.; Staroverov, V. N.; Kobayashi, R.; Normand, J.; Raghavachari, K.; Rendell, A.; Burant, J. C.; Iyengar, S. S.; Tomasi, J.; Cossi, M.; Rega, N.; Millam, J. M.; Klene, M.; Knox, J. E.; Cross, J. B.; Bakken, V.; Adamo, C.; Jaramillo, J.; Gomperts, R.; Stratmann, R. E.; Yazyev, O.; Austin, A. J.; Cammi, R.; Pomelli, C.; Ochterski, J. W.; Martin, R. L.; Morokuma, K.; Zakrzewski, V. G.; Voth, G. A.; Salvador, P.; Dannenberg, J. J.; Dapprich, S.; Daniels, A. D.; Farkas, Ö.; Foresman, J. B.; Ortiz, J. V.; Cioslowski, J.; Fox, D. J. Gaussian, Inc.: Wallingford CT, 2009.
(73) Fumino, K.; Peppel, T.; Geppert-Rybczynska, M.; Zaitsau, D. H.; Lehmann, J. K.; Verevkin, S. P.; Köckerling, M.; Ludwig, R. *Phys. Chem. Chem. Phys.* **2011**, *13*, 14064.